International Journal of Greenhouse Gas Control 5 (2011) 1507–1516

Contents lists available at SciVerse ScienceDirect

International Journal of Greenhouse Gas Control

journal homepage: www.elsevier.com/locate/ijggc

He and Ne as tracers of natural CO_2 migration up a fault from a deep reservoir

Stuart M.V. Gilfillan[a,*], Mark Wilkinson[a], R. Stuart Haszeldine[a], Zoe K. Shipton[b], Steven T. Nelson[c], Robert J. Poreda[d]

[a] Scottish Carbon Capture and Storage, School of GeoSciences, The University of Edinburgh, Grant Institute, The King's Buildings, West Mains Road, Edinburgh, EH9 3JW, UK
[b] Department of Civil Engineering, University of Strathclyde, Glasgow, Scotland, G1 1XU, UK
[c] Department of Geological Sciences, Brigham Young University, S-389 ESC, Provo, UT 84602, USA
[d] Department of Earth and Environmental Sciences, University of Rochester, Rochester, NY 14627, USA

ARTICLE INFO

Article history:
Received 27 January 2011
Received in revised form 8 August 2011
Accepted 12 August 2011
Available online 14 September 2011

Keywords:
Carbon capture and storage
Geochemical tracing of CO_2
Noble gases
Carbon isotopes
Geological storage of CO_2
Natural analogues

ABSTRACT

Capture and geological storage of CO_2 is emerging as an attractive means of economically abating anthropogenic CO_2 emissions from point sources. However, for the technology to be widely deployed it is essential that a reliable means to assess a site for both storage performance and regulation compliance exists. Hence, the ability to identify the origin of any CO_2 seepage measured at the near-surface and ground surface and determine if it originates from a deep storage site or a different source is critical. As an analogue for post-emplacement seepage, here we examine natural CO_2 rich springs and groundwater wells in the vicinity of the St. Johns Dome CO_2 reservoir located on the border of Mid-Arizona/New Mexico, USA. Extensive travertine deposits in the region document a long history of migration of CO_2 rich fluids to the surface. The presence of CO_2 rich fluids today are indicated by high levels of HCO_3^- in surface spring and groundwater well waters. We document measurements of dissolved noble gases and carbon isotopes from these springs and wells. We show that a component of the He fingerprint measured in gaseous CO_2 sampled in the deep reservoir, can be traced along a fault plane to occur in waters from both groundwater wells and the majority of springs emerging at the surface above the reservoir. Our results show for the first time that CO_2 can be fingerprinted from source to surface using noble gases and illustrates that this technique could be used to identify dissolved CO_2 migration from engineered storage sites.

1. Introduction

Engineered CO_2 storage sites consist of both the formation (reservoir) into which CO_2 is injected, and the overlying primary seal, together with the suite of rocks above the site up to the ground surface (overburden). In the recent EU directive on the geological storage of CO_2, the overburden is legally defined as part of the "storage complex" (E.U., 2009), and hence its containment performance needs to be evaluated to ensure that CO_2 can be stored over geological timescales. It is extremely difficult to unequivocally detect the small releases of anthropogenic CO_2 that could arise from a diffuse leakage of CO_2 from a storage site. This is because there are many natural sources of CO_2 within the crust with overlapping signatures, including breakdown of carbonate minerals or cements, biological activity or hydrocarbon oxidation (Wycherley et al., 1999). Predictions made by laboratory measurements and computational simulations of gas movement require scale-up and validation by natural examples as the pathways and processes affecting CO_2 migration through overburden are presently poorly understood (Benson and Hepple, 2005). Few studies have investigated tracing CO_2 migration through overburden to the subsurface (Wildenborg et al., 2005). In order to provide reassurance to both regulators and the public that a CO_2 leak could be identified, a specific and unambiguous method is needed to trace the migration of deep-derived CO_2 from depth to the surface. One option is to use the naturally occurring gas tracers within the CO_2, such as the noble gases (Wilkinson et al., 2010), or the isotope ratios of the carbon and oxygen contained in the CO_2 (Fessenden et al., 2010; Krevor et al., 2010). Another option is to add artificial gas tracers such as SF_6 or specific noble gases such as Kr and Xe (Nimz and Hudson, 2005). However it is not yet known if the 'fingerprints' provided by these natural and artificial tracers will remain intact during the diverse geochemical and petrophysical interactions that occur as CO_2 migrates. Here, at St Johns, we show that the He fingerprint measured in deep reservoir CO_2 is transmitted to the water containing dissolved CO_2 at the surface.

Noble gases are extremely powerful tracers of source and the subsurface processes that act on CO_2 (Ballentine et al., 2001, 2002; Sherwood Lollar and Ballentine, 2009; Sherwood Lollar et al., 1994, 1997). This is because there are three distinct sources of noble

* Corresponding author. Tel.: +44 0131 650 7010.
E-mail address: stuart.gilfillan@ed.ac.uk (S.M.V. Gilfillan).

1750-5836/$ – see front matter © 2011 Elsevier Ltd. All rights reserved.
doi:10.1016/j.ijggc.2011.08.008

gases within the subsurface, namely the crust, mantle and the atmosphere. Crustal noble gases, such as ^{4}He and ^{40}Ar, are produced by the radioactive decay of uranium, thorium and potassium within the crust (Ballentine and Burnard, 2002). Mantle derived noble gases, such as ^{3}He, were trapped within the mantle during the accretion of the Earth and have been degassing ever since (Ballentine and Burnard, 2002). Atmospheric noble gases, such as ^{20}Ne and ^{36}Ar enter the subsurface dissolved in the groundwater via meteoric recharge (Ballentine and Burnard, 2002). The distinct elemental and isotopic composition of these three noble gas components allows the contribution from each source to be determined and provides detailed information on the source and transport processes associated with the CO_2 (Ballentine, 1991; Ballentine et al., 2002; Sherwood Lollar and Ballentine, 2009).

Noble gases have been widely used to trace regional flows of groundwater in numerous locations (Castro and Goblet, 2003; Castro et al., 1998). Recent studies have successfully demonstrated the potential of noble gases to trace the origins of CO_2 and its fate within reservoirs (Gilfillan et al., 2008, 2009; Lafortune et al., 2009; Nimz and Hudson, 2005). However, there has not yet been a successful demonstration that noble gases can be used to trace diffuse CO_2 migration through the subsurface to the surface at an individual site. In order to conclusively determine if migration of dissolved CO_2 is responsible for the high HCO_3^- concentrations measured in both surface and well waters at St. Johns, we compare a suite of noble gas and stable isotope tracers measured in CO_2 from the deep St. Johns CO_2 reservoir to those measured in spring and well waters. We also use these tracers to determine if there is evidence of a preferential migration pathway of dissolved CO_2 through the overburden.

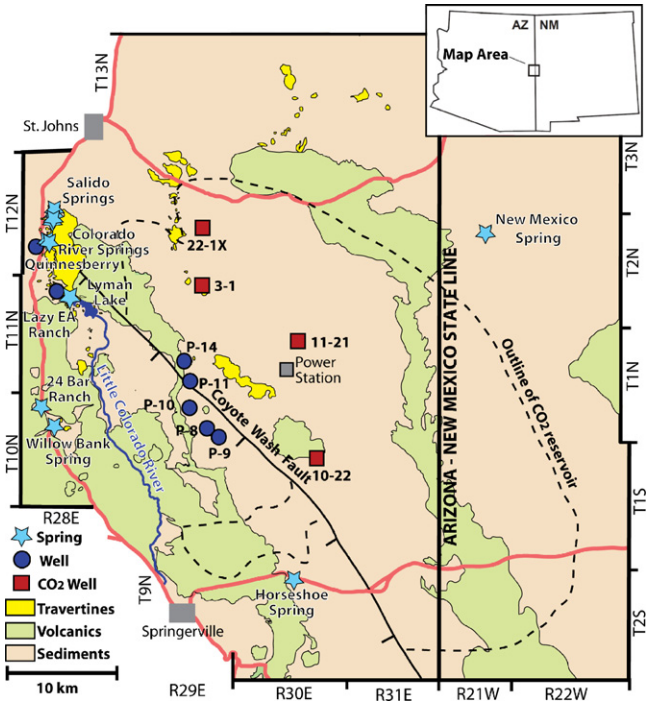

Fig. 1. Simplified geological map of the St. Johns–Springerville area. Inset: Location of the map in relation to the states of Arizona and New Mexico, USA. Outlined on the map is the base of the reservoir boundary, at 1494 m, the trace of the major Coyote Wash fault and the location of travertine and volcanic deposits. Also shown are the CO_2 wells, groundwater wells and surface spring samples collected for this study. Redrawn from Moore et al. (2005) and Sirrine (1956).

2. Geological setting of St. Johns Dome

The St. Johns Dome CO_2 reservoir is located on the south eastern edge of the Holbrook basin, on the border of Arizona and New Mexico. This is within the transition zone between the Colorado Plateau, Basin and Range and Rio Grande Rift tectonic provinces. The reservoir is comprised of a broad symmetrical northwest-trending anticline at the northeast tip of the Springerville Volcanic field (Fig. 1).

The Springerville Volcanic field covers nearly 3000 km^2 and is believed to have been formed from 300 km^3 of lava from some 400 volcanic centres. This is one of many late Pliocene to Holocene, predominantly basaltic, volcanic fields which surrounds the southern margin of the Colorado Plateau (Baars, 2000).

The CO_2 in the St. Johns Dome reservoir is contained in the Permian Supai Formation which is predominantly a fine-grained alluvial sandstone intercalated with siltstone, anhydrite and dolomite. The field is estimated to contain 445 billion m^3 of CO_2 (Stevens et al., 2006). The reservoir is dissected by a steeply dipping northwest–southeast tending major fault, named the Coyote Wash fault (Rauzi, 1999). The cap rock consists of impermeable anhydrites which vertically separate the CO_2 into multiple zones. The reservoir is relatively shallow at 200–700 m and the CO_2 is present in a gas state. CO_2 is contained primarily in the Fort Apache Limestone Member, Big A Butte Member and Amos Wash member of the Permain Supai Formation. The average reservoir porosity is 10% and permeability varies widely from 0.5 to 100 mD, averaging 10 mD (Stevens et al., 2006). No igneous or volcanics were cored during exploration of the field (Rauzi, 1999).

The St. Johns–Springerville region contains one of the largest concentrations of travertine deposits in the U.S. These cover an area of approximately 250 km^2, predominantly south and east of the town of St. Johns. The travertine deposits are particularly concentrated in a 10 km long zone between Lyman Lake and Salado Springs (Fig. 1) located at the tip of the Coyote Wash Fault. Cold water springs (less than 10 °C above ambient temperature) are also associated with these travertine deposits and suggest that the Coyote Wash fault is influencing the groundwater hydrological regime in the region (Crumpler et al., 1994). The largest sheet of travertine is some 6.4 by 3.2 km in size and numerous circular dome deposits are also present. These typically contain central chambers marking the locations of the spring vents (Moore et al., 2005). The largest of these deposits is some 600 m in diameter and 50 m in height.

It is believed that travertine deposition commenced during the late Pleistocene as the oldest deposits postdate the basaltic volcanism of the Springerville Volcanic field and are interbedded with late Pleistocene gravels of the Richville formation (Sirrine, 1956). The oldest presumed travertine deposits are found to the south east of Lyman Lake (Fig. 1) and these are some 325 m above the current level of the Little Colorado River (Moore et al., 2005). This is similar to extinct travertine deposits at Green River in central Utah which are found several tens of metres above the current active springs at river level (Dockrill and Shipton, 2010). The rate of erosion in tributaries of the Colorado River in central and southern Utah range from ~20 to 40 cm per thousand years (Baer and Rigby, 1978; Doelling, 1994). It is thought that similar erosion rates are likely for the St. Johns Springerville region (Moore et al., 2005). Using these erosion rates and assuming that the differences in elevation are the result of erosion and a consequent change in the base level of the river then the age of the oldest travertine deposits ranges from 0.81 to 1.6 Ma years ago. However, as field evidence indicates that the oldest travertine deposits are of late Pleistocene age, there must be additional factors, such as intermittent pulses of CO_2 or faulting, controlling the temporal and spatial fluctuations in travertine formation.

Whilst the size and predominance of these deposits implies an extensive history of CO_2 rich fluid leakage, many of the domes

Table 1
Sample location, feature, field conditions, HCO_3^- and noble gas concentrations, $\delta^{13}C$ (CO_2), $\log P_{CO_2}$ and $CO_2/^3He$ ratios.

Sample	Location (UTM zone 12)	Feature	Depth (m)	pH	Temp (°C)	HCO_3 (mg l^{-1})	^3He ($\times10^{-10}$), $cm^3(STP)cm^{-3}$	^4He ($\times10^{-4}$), $cm^3(STP)cm^{-3}$	^{20}Ne ($\times10^{-5}$), $cm^3(STP)cm^{-3}$	^{40}Ar ($\times10^{-2}$), $cm^3(STP)cm^{-3}$	$\delta^{13}C_{DIC}$ (‰)	$\log P_{CO_2}$	$CO_2/^3He$ ($\times10^9$)
Horseshoe Spring	667996 3781127	Surface Spring	0	7.8	10.1	304	1.52 (2)	1.27 (2)	0.773 (20)	2.03 (2)	−12.0 (2)	−2.37	0.751 (7)
Willow Bank Spring	647233 3793618	Surface Spring	0	6.9	16.2	142	0.0698 (8)	0.0469 (5)	2.47 (7)	2.68 (3)	−10.0 (2)	−1.76	10.6 (1)
24 Bar Ranch	646044 3795443	Surface Spring	0	7.0	14.4	146	0.187 (1)	0.131 (2)	4.79 (13)	1.87 (2)	−7.00 (2)	−1.87	3.66 (4)
New Mexico Spring[a]	683664 3810437	Surface Spring	0	9.6	19.3	200.0	0.205 (1)	0.132 (2)	4.40 (12)	1.43 (2)	–	−4.62	3.94 (4)
Colorado River Dome	646776 3809069	Surface Spring	0	6.1	17.9	–	23.3 (1)	19.4 (2)	4.59 (12)	1.80 (2)	–	–	–
Colorado River Spring[a]	646698 3809228	Surface Spring	0	7.2	15.6	75.0	11.0 (1)	10.7 (1)	5.42 (14)	2.40 (3)	–	−2.45	0.0283 (3)
Lyman Lake Spring	648393 3804131	Surface Spring	0	6.9	6.9	744	3.01 (2)	2.77 (3)	3.13 (8)	2.62 (3)	−8.5 (2)	−1.15	1.18 (1)
Salido Springs 1	647138 3811498	Surface Spring	0	6.7	13.2	724.5	1.97 (1)	2.29 (2)	2.41 (6)	2.33 (3)	−0.6 (2)	−0.95	1.94 (2)
Salido Springs 2	647131 3811487	Surface Spring	0	6.6	18.4	712.4	7.46 (4)	8.42 (9)	4.22 (11)	2.44 (3)	−0.4 (2)	−0.87	0.521 (5)
Salido Springs 3	647112 3811409	Surface Spring	0	6.9	19.1	–	3.53 (2)	4.19 (4)	3.95 (10)	2.64 (3)	–	–	–
Salido Springs 4	647082 3810841	Surface Spring	0	6.3	19.5	–	3.23 (2)	3.74 (4)	3.17 (8)	2.29 (3)	–	–	–
P-8	660451 3793613	Power Station Well	357	6.9	24.8	506.0	5.99 (3)	5.46 (6)	1.49 (4)	1.47 (2)	−4.5 (2)	−1.26	0.393 (4)
P-9	661478 3792894	Power Station Well	369	6.7	25.9	646.8	20.6 (1)	16.1 (2)	2.67 (7)	2.06 (2)	−0.1 (2)	−0.95	0.161 (2)
P-10[b]	658972 3795316	Power Station Well	419	7.5	23.8	556.4	25.9 (2)	20.6 (2)	4.99 (13)	2.17 (2)	−0.5 (2)	−1.84	0.0853 (9)
P-11[b]	658992 3797558	Power Station Well	434	7.2	24.3	471.7	17.2 (1)	14.6 (2)	4.85 (13)	2.29 (3)	−1.9 (2)	−1.59	0.115 (2)
P-14	658521 3798929	Power Station Well	441	6.6	25.9	691.4	14.1 (1)	17.3 (2)	2.54 (7)	1.90 (2)	0.9 (2)	−0.78	0.142 (2)
Quisenberry-1	645713 3808636	Irrigation Well	94	6.9	13.6	431.0	15.3 (1)	14.3 (2)	3.16 (8)	2.49 (3)	−11.3 (2)	−1.36	0.133 (2)
Quisenberry-2	647138 3811498	Irrigation Well	94	6.9	13.6	431.0	27.7 (2)	24.1 (3)	4.32 (11)	2.28 (2)	−11.3 (2)	−1.36	0.0735 (7)
Lazy EA Ranch	647602 3804940	Irrigation Well	12	7.0	13.3	–	5.98 (3)	5.93 (6)	5.01 (13)	2.58 (2)	–	–	–
11-21	667945 3800940	Gas Well	735	7.1	30.1	1190.0	–	–	–	–	–	−1.07	–
22-1X	659725 3810442	Gas Well	655	–		–	85.1 (1.5)	134 (1)	0.0344 (5)	0.259 (14)	−3.6 (2)	–	0.098 (2)
10-22	669730 3791327	Gas Well	690	–		–	5.18 (9)	9.42 (9)	0.00230 (3)	0.0252 (13)	−3.8 (2)	–	1.91 (4)
3-1	659807 3805620	Gas Well	553	–		–	42.7 (8)	70.6 (7)	0.0151 (2)	0.117 (6)	−3.8 (2)	–	0.22 (3)

$^3He/^4He$ are corrected for air contributions (Craig et al., 1978). 24 Bar Ranch, New Mexico and Willow Bank springs cannot be corrected due to tritogenic ^3He.

[a] These springs were not re-sampled for this study, HCO_3^- values are from Moore et al. (2005).

[b] Due to operational reasons these wells were not re-sampled for $\delta^{13}C$ and HCO_3^- so P-15 was sampled in place of P-10 and P-16 for P-11.

are now dry and it appears that current travertine deposition is extremely limited or non-existent. All of the flowing groundwater springs are less than 3 m above the elevation of the Little Colorado River, implying that the local groundwater table is controlling the outflow (Moore et al., 2005). None of the springs or pools, surveyed in 2006, where actively exsolving CO_2 indicating the partial pressure of CO_2 must be less than 1 bar. Nevertheless, high concentrations of HCO_3^- are common in surface springs, shallow groundwater wells used for irrigation, and deeper wells used to obtain cooling water for a coal fired power plant in the region (Table 1). Previous chemical analysis of these waters indicated a possible connection between the formation water within the deep CO_2 reservoir and these shallow HCO_3^- rich waters (Moore et al., 2005). However, this link is not conclusive, due to significant differences in water types (Moore et al., 2005) and as a soil gas flux survey surrounding these springs and wells was unable to differentiate any additional CO_2 flux from that of background biological activity (Allis et al., 2005).

3. Sample collection and analytical techniques

$\delta^{13}C$ (CO_2) isotopes, noble gas composition and isotope ratios for the CO_2 reservoir samples are from Gilfillan et al. (2008, 2009). CO_2 samples from the St. Johns Dome reservoir were collected in Swagelok® 300 ml stainless steel sampling cylinders fitted at both ends with two high-pressure valves. All cylinders were baked at 150 °C under vacuum before being shipped to the field. The cylinders were attached directly to the sampling port of the wellhead prior to the gas undergoing any form of commercial processing. A 20 cm length of high pressure hosing was attached to the other end of the cylinder as an exhaust to prevent turbulent back mixing. The cylinders were flushed through with gas from the wellhead for 5 min before the outer valve was shut and the cylinder equilibrated at wellhead pressure, which ranged from 1.93 to 3.44 MPa. The cylinder valve closest to the well head was then shut and the gas vented by opening the outer cylinder valve. This valve was closed before complete positive pressure was lost. This purge procedure was repeated 5 more times before all valves were closed sequentially, from the outer valve to the valve closest to the sampling port, in order to collect the sample at wellhead pressure (Gilfillan et al., 2008).

Water samples for noble gas analysis were collected from five groundwater wells producing water for the Springerville Generating Station coal fired power plant, two agricultural irrigation wells and eleven surface springs from the St. Johns Springerville region in the Autumn of 2006. Sampling localities are shown in Fig. 1. Water samples were collected using a copper tube technique similar to the method used for gas sampling at McElmo Dome outlined in Gilfillan et al. (2008). For both the power station wells and the irrigation well samples, water was pumped directly from the well head via high pressure hosing through a length of copper tube. Water was pumped for a period of 5 min to flush out any atmospheric contamination. The copper tube clamp furthest from the well head was then closed, followed by the remaining clamp ensuring that the copper was cold welded to form a leak tight, sealed water sample for analysis. All of the surface springs were associated with deep pools of water (>1 m in depth). Water samples from these pools were collected using a peristaltic pump and a weighted 1 m length of high pressure hosing. This was to ensure that no atmospheric contamination was induced by pumping the water from the spring and that the water was collected from the deeper portions of the pool closer to the input, further limiting atmospheric contamination. As with the well water samples, water was pumped for 5 min as further measure to reduce atmospheric contributions. The copper tube clamp furthest from the pump was then closed, followed by the remaining clamp ensuring that the copper was cold welded to form a leak tight sealed water sample for analysis.

Water samples for $\delta^{13}C_{DIC}$ and water composition analysis were collected in spring 2007. Samples were collected from one of the irrigation wells, four of the groundwater springs and from six of the power station wells. Due to time constraints not all of the localities sampled for noble gases were also sampled for stable isotopes and water composition. However Moore et al. (2005) completed extensive water composition analysis in the area and we use this water composition data for two springs that were not re-sampled (New Mexico Spring and Colorado River Spring). Details of the sampling and analysis of these samples is documented in Moore et al. (2005). Additionally, because of operational reasons only three of the five power station wells sampled for noble gases were re-sampled (TEP-10 and TEP-11 were not). However, nearby wells which source water from the same aquifer were collected (TEP-15 and TEP-16) and these are used to provide composition data for these wells. Lazy EA ranch was not re-sampled due to access restrictions.

Isotopic ratios ($^3He/^4He$, $^{20}Ne/^{22}Ne$, $^{21}Ne/^{22}Ne$, $^{40}Ar/^{36}Ar$, $^{38}Ar/^{36}Ar$) and elemental abundances (^4He, ^{20}Ne, ^{40}Ar) were determined on the University of Rochester's VG 5400 mass spectrometer, using the techniques outlined in (Poreda and Farley, 1992). The 2δ analytical error for the $^3He/^4He$ ratio is 0.5% and those for both the $^{40}Ar/^{36}Ar$ and $^4He/^{20}Ne$ isotope ratios were 0.2%, and 0.3% for $^{38}Ar/^{36}Ar$. Helium isotope ratios ($^3He/^4He$) are expressed relative to the ratio in air ($R_a = R_{measured}/R_{air}$ where $R_{air} = 1.399 \times 10^{-6}$). All other ratios are absolute values. All gas concentrations are corrected to standard temperature and pressure (STP).

$\delta^{13}C$ analysis for dissolved gas was undertaken at Brigham Young University (BYU). Anion concentrations other than bicarbonate (measured by titration) were also determined at BYU using a Dionex ICS-90 ion chromatograph. Cation abundances were measured with a Perkin Elmer 5100C Atomic Absorption Spectrometer. The acceptable charge balance error was ≤5%. One dissolved inorganic carbon [DIC] sample, quantitatively precipitated as $BaCO_3$ and acidified (McCrea, 1950), and one exsolved CO_2 gas sample were analyzed at BYU against an NBS-19 calibrated reference gas. Results are expressed relative to the V-PDB standard.

Using the chemical composition, temperature and pH of the water samples, the maximum concentration of CO_2 in the samples under the measured physical and geochemical conditions was modelled. PHREEQC (Parkhurst and Appelo, 1999) was used to calculate a description of each solution which was equilibrated with excess CO_2 (50 atmospheres) and in equilibrium with calcite, in order to calculate the total dissolved CO_2 concentration in mol/kg. This was used to calculate the mass of CO_2 per kg, CO_2 volume per kg at STP and at measured conditions and the concentration of CO_2 in each sample using water density values corrected for salinity. Combining these values with the measured ^3He concentrations provided the $CO_2/^3He$ ratios.

4. Results

Table 1 documents the sample location, feature, depth, pH, temperature, HCO_3^- and noble gas concentrations (^4He, ^{20}Ne, ^{40}Ar), $\delta^{13}C_{DIC}$ isotopes, $\log P_{CO_2}$ and $CO_2/^3He$ ratios. Table 2 outlines the noble gas isotopic ratio measurements ($^3He/^4He$, $^{20}Ne/^{21}Ne$, $^{21}Ne/^{22}Ne$ $^{40}Ar/^{36}Ar$, $^{38}Ar/^{36}Ar$, $^4He/^{20}Ne$ and $^{20}Ne/^{36}Ar$) and the chemical analysis of water samples collected for this study (Ca, Mg, Na, K, HCO_3, CO_3, F, Cl, NO_3, Br SO_4 and TDS).

4.1. $\delta^{13}C$ (CO_2) and $\delta^{13}C_{DIC}$ isotopes

Measured $\delta^{13}C$ (CO_2) isotopes within the three deep reservoir CO_2 wells exhibit an extremely small range from −3.6 to −3.8‰, with the lowest value being observed in the southern portion of the

Table 2
Noble gas ratios and chemical composition of water samples. All composition values are in mgl^{-1}.

Sample	$^3He/^4He_c$ (R/R_a)	$^{20}Ne/^{22}Ne$	$^{21}Ne/^{22}Ne$	$^{40}Ar/^{36}Ar$	$^{38}Ar/^{36}Ar$	$^4He/^{20}Ne$	$^{20}Ne/^{36}Ar$	Ca	Mg	Na	K	CO_3	F	Cl	NO_3	Br	SO_4	TDS
Horseshoe Spring	0.849 (4)	9.86 (2)	0.0290 (1)	299 (1)	0.191 (1)	16.5 (5)	0.114 (2)	64.6	21.7	21.5	3.1	0.00	0.4	27.6	0.77	1.32	20.0	464.5
Willow Bank Spring	1.064 (5)	9.81 (2)	0.0290 (1)	296 (1)	0.187 (1)	0.19 (1)	0.273 (4)	20.1	10.7	12.1	3.8	0.00	0.1	8.3	2.53	0.00	8.1	208.1
24 Bar Ranch	1.015 (5)	10.02 (2)	0.0292 (1)	297 (1)	0.188 (1)	0.27 (1)	0.761 (11)	20.2	12.1	11.1	4.8	0.00	0.1	4.6	0.72	0.00	5.9	205.4
New Mexico Spring[a]	1.106 (6)	9.97 (2)	0.0290 (1)	293 (1)	0.189 (1)	0.30 (1)	0.900 (13)	30.0	30.0	290.0	20.0	18.0	–	65.0	–	0.00	–	–
Colorado River Dome	0.858 (4)	10.03 (2)	0.0292 (1)	299 (1)	0.186 (1)	42.4 (1.2)	0.760 (11)	–	–	–	–	–	–	–	–	–	–	–
Colorado River Spring[a]	0.729 (4)	9.96 (2)	0.0290 (1)	299 (1)	0.189 (1)	19.7 (6)	0.677 (10)	310.0	70.0	380.0	25.0	<0.10	–	420.0	–	0.00	65.0	2308.0
Lyman Lake Spring	0.770 (4)	9.96 (2)	0.0291 (1)	297 (1)	0.189 (1)	8.8 (3)	0.354 (5)	82.2	42.7	194.4	10.8	0.00	2.4	68.2	0.22	2.23	149.0	1296.4
Salido Springs 1	0.535 (3)	9.94 (2)	0.0292 (1)	297 (1)	0.191 (1)	9.5 (3)	0.308 (4)	337.4	46.9	319.1	27.1	0.00	2.0	432.0	0.22	0.00	671.9	2561.3
Salido Springs 2	0.627 (3)	10.02 (2)	0.0291 (1)	297 (1)	0.188 (1)	20.0 (6)	0.514 (7)	339.0	46.0	318.0	27.0	0.00	2.0	427.8	0.00	0.00	–	–
Salido Springs 3	0.523 (3)	9.98 (2)	0.0291 (1)	296 (1)	0.188 (1)	10.6 (3)	0.442 (6)	–	–	–	–	–	–	–	–	–	–	–
Salido Springs 4	0.539 (3)	10.03 (2)	0.0291 (1)	296 (1)	0.189 (1)	11.8 (3)	0.410 (6)	–	–	–	–	–	–	–	–	–	–	–
P-8	0.782 (4)	9.93 (2)	0.0289 (1)	299 (1)	0.186 (1)	36.5 (1.0)	0.304 (4)	178.7	41.4	178.5	16.1	0.00	1.9	220.1	0.00	0.00	355.9	1498.6
P-9	0.915 (5)	10.05 (2)	0.0289 (1)	302 (1)	0.187 (1)	60.4 (1.7)	0.391 (6)	284.4	40.1	267.0	22.5	0.00	2.0	362.5	0.00	0.00	532.2	2157.5
P-10	0.982 (5)	9.99 (2)	0.0289 (1)	300 (1)	0.188 (1)	41.2 (1.2)	0.690 (10)	190.3	42.6	198.7	17.0	0.00	2.0	253.4	0.22	0.00	393.2	1653.7
P-11	0.841 (4)	9.98 (2)	0.0290 (1)	298 (1)	0.192 (1)	30.2 (9)	0.630 (9)	154.3	39.1	142.0	13.5	0.00	2.0	170.7	0.21	0.00	285.5	1279.1
P-14	0.581 (3)	10.01 (2)	0.0290 (1)	307 (1)	0.197 (1)	68.1 (1.9)	0.410 (6)	335.5	54.0	102.2	28.0	0.00	2.1	251.2	0.00	0.00	382.3	1846.6
Quisenberry-1	0.766 (4)	9.93 (2)	0.0291 (1)	300 (1)	0.187 (1)	45.1 (1.3)	0.380 (5)	4.3	6.3	395.9	22.0	0.00	1.1	410.5	0.29	0.00	29.0	1300.4
Quisenberry-2	0.820 (4)	9.96 (2)	0.0289 (1)	303 (1)	0.190 (1)	55.8 (1.6)	0.575 (8)	4.3	6.3	395.9	22.0	0.00	1.1	410.5	0.29	0.00	29.0	1300.4
Lazy EA Ranch	0.713 (4)	9.98 (2)	0.0290 (1)	301 (1)	0.188 (1)	11.8 (3)	0.585 (8)	–	–	–	–	–	–	–	–	–	–	–
11-21 State	–	–	–	–	0.191 (1)	–	–	110.0	232.0	804.0	174.0	–	0.0	483.0	–	–	1540.0	4210.0
22-1X	0.455 (11)	9.75 (9)	0.0408 (2)	1369 (13)	0.197 (2)	38.855 (646)	0.182 (6)	–	–	–	–	–	–	–	–	–	–	–
10-22	0.393 (10)	9.71 (11)	0.0446 (2)	1492 (15)	0.197 (3)	40.897 (682)	0.136 (5)	–	–	–	–	–	–	–	–	–	–	–
3-1	0.432 (11)	9.80 (3)	0.0420 (3)	1687 (16)	0.187 (4)	46.651 (778)	0.219 (8)	–	–	–	–	–	–	–	–	–	–	–

[a] These springs were not re-sampled for this study so water composition data is from Moore et al. (2005).

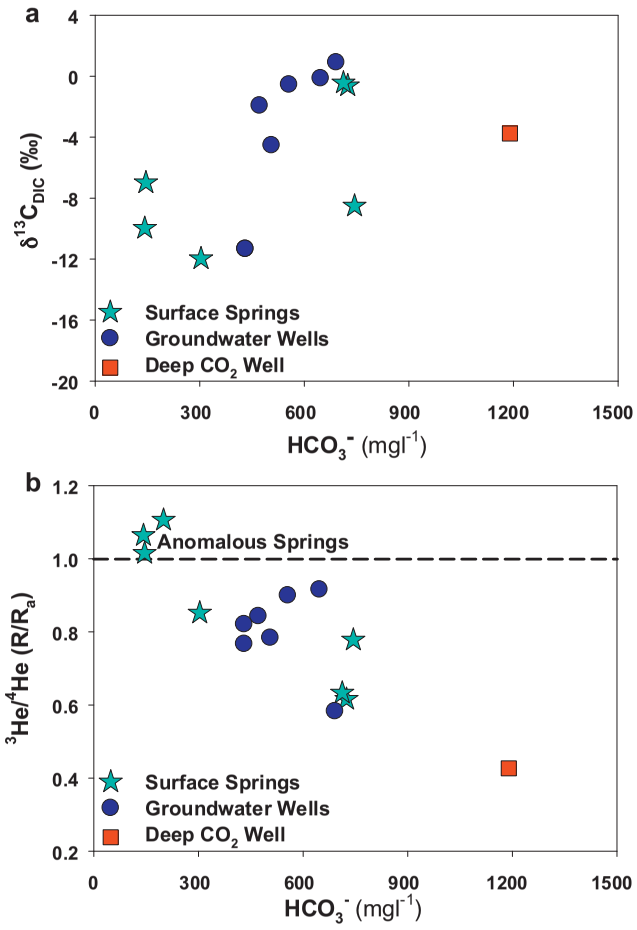

Fig. 2. (a) $\delta^{13}C_{DIC}$ variation plotted against HCO_3^- concentrations for the surface springs, groundwater and CO_2 wells sampled. The calculated mean $\delta^{13}C(CO_2)$ value for the CO_2 reservoir was converted into $\delta^{13}C_{DIC}$ using the gas to DIC fractionation factor previously calculated for St. Johns Dome (Gilfillan et al., 2009). There is no clear relationship between the HCO_3^- concentration of the water and $\delta^{13}C_{DIC}$ or the sample type. (b) $^3He/^4He$ ratios plotted against HCO_3^- concentrations for the surface springs, groundwater wells and CO_2 well sampled. The black dash line indicates the air $^3He/^4He$ value of 1. There is a clear distinction between the above air ratios measured in three anomalous spring water samples; Willowbank Spring, 24 Bar Ranch and New Mexico Spring, caused by the addition of tritiogenic ^3He and the below air $^3He/^4He$ ratios measured in the other samples. There is also a correlation between increasing HCO_3^- concentrations and $^3He/^4He$ decreasing towards the values measured in the deep CO_2 reservoir.

reservoir. The mean $\delta^{13}C(CO_2)$ isotope value of the reservoir CO_2 of −3.7‰ was converted to $\delta^{13}C_{DIC}$ using the CO_2 gas to DIC fractionation factor of 0.02‰ for St. Johns Dome calculated in Gilfillan et al. (2009). This allows direct comparison of the deep CO_2 reservoir water $\delta^{13}C_{DIC}$ value with those measured in the well and surface waters (Fig. 2a).

The water samples exhibit a large range of values, from −12.0‰ (Horseshoe Spring) to 0.9‰ (P-14). The five power station wells show a smaller range (between 0.9 to −4.53) than the other water samples which show no correlation between the $\delta^{13}C(CO_2)$ isotope value and sample type (Fig. 2a).

4.2. Helium

Measured $^4He/^{20}Ne$ ratios in all samples bar Willow Bank, 24 Bar Ranch and New Mexico Springs (hereafter known as the anomalous springs) are above the calculated air ratio of 0.26 indicating that atmospheric He contributions to all samples bar these three is minimal (Fig. 3).

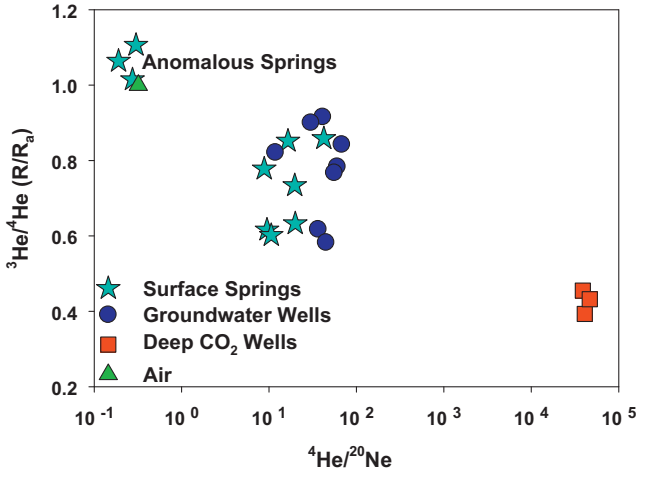

Fig. 3. $^{3}He/^{4}He$ plotted against $^{4}He/^{20}Ne$. The lower $^{3}He/^{4}He$ measured in all of the deep groundwater wells and majority of surface springs (excluding 24 Bar Ranch, New Mexico and Willow Bank springs) corresponds to significantly higher $^{4}He/^{20}Ne$ indicating the presence of excess ^{4}He from depth. The air like $^{4}He/^{20}Ne$ (calculated air ratio of 0.26) of 24 Bar Ranch, New Mexico and Willow Bank springs further indicates that these springs do not contain excess ^{4}He.

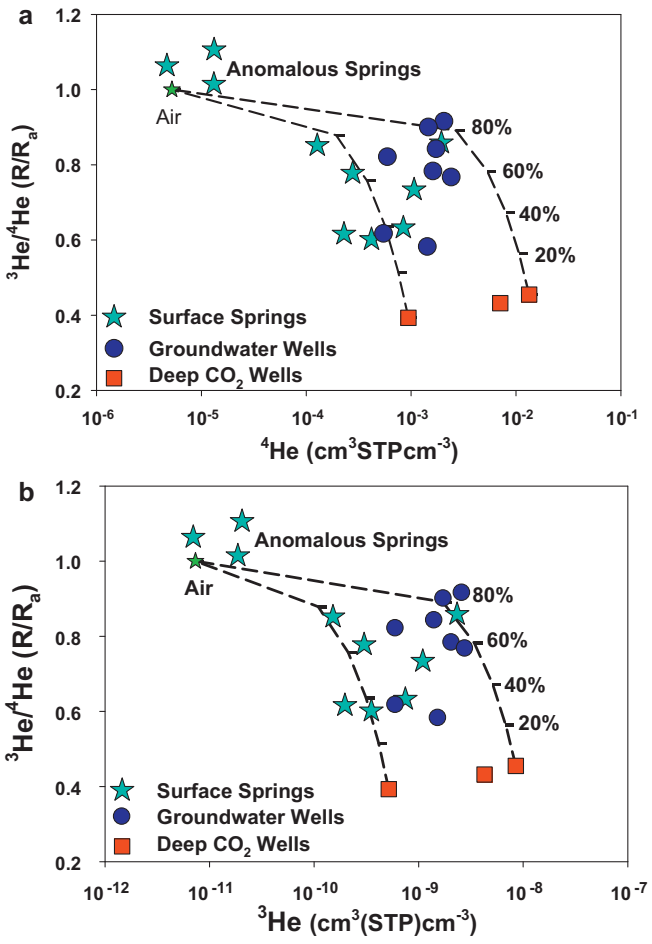

Fig. 4. (a) ^{4}He plotted against $^{3}He/^{4}He$, with mixing lines plotted from different compositions of deep groundwater measured from wells, to 100% air. The low $^{3}He/^{4}He$ and high ^{4}He within the groundwater wells and majority of surface springs can be explained by simple mixing between the $^{3}He/^{4}He$ and ^{4}He values measured in wells 10-22 and 22-1X and varying amounts of air (percent air indicated on tick marks). This proves that the excess ^{4}He component entrained at depth is retained and not lost on migration of the waters to the surface. (b) ^{3}He plotted against $^{3}He/^{4}He$. As with ^{4}He, the high ^{3}He concentrations and low $^{3}He/^{4}He$ ratios observed in the groundwater wells and the majority of the surface springs can be accounted by mixing of the values measured in wells 10-22 and 22-1X and varying amounts of air. This shows that the high magmatic ^{3}He signature exhibited by the deep CO_2 wells, although diluted, is retained and not lost as a result of transport water to the surface.

The lowest $^{3}He/^{4}He$ ratios are those measured in the three deep gas wells from the St. Johns CO_2 reservoir (Fig. 2b). These range from $0.39R_a$ (well 10-22) to $0.46R_a$ (well 22-1X) on moving towards the gas/formation water contact towards the south of the reservoir. Within subsurface fluid samples the $^{3}He/^{4}He$ ratio is typically dependent on the variation in crustal ^{4}He contribution (Ballentine et al., 2002). However in the St. Johns reservoir this increase in $^{3}He/^{4}He$ ratio is somewhat surprising given that ^{4}He concentrations correspondingly increase, opposite to what would be expected if the $^{3}He/^{4}He$ ratio was being controlled solely by ^{4}He concentration. This could be explained by the presence of a significant magmatic ^{3}He component within the regional formation water, not just in the CO_2 (Gilfillan et al., 2008). This would result in a high regional $^{3}He/^{4}He$ ratio in the formation water. This He, with a high $^{3}He/^{4}He$, could then be degassed from the formation water at the gas/water contact by the same mechanism that is degassing the formation water-derived ^{20}Ne, ^{36}Ar and crustal N_2 concentrations within the reservoir (Gilfillan et al., 2008).

$^{3}He/^{4}He$ ratios in the both the power station and agricultural water wells vary from 0.58 (P-14) to 0.92 (P-9) R_a. However, $^{3}He/^{4}He$ ratios do not correlate directly to either ^{3}He or ^{4}He concentrations (Fig. 4). The three anomalous springs which display air like $^{4}He/^{20}Ne$ ratios also exhibit $^{3}He/^{4}He$ ratios above the air ratio (Fig. 2b). This is due to the presence of tritogenic He, originating from the copious amounts of tritium released into the atmosphere as a result of nuclear weapons testing from the 1950s to 1980s (Happell et al., 2004). This indicates that the water emanating from these springs is less than 50 years old. This clearly distinguishes these springs from the other eight springs that exhibit a $^{3}He/^{4}He$ ratio range of 0.60 (Salido Springs 4) to $0.86R_a$ (Little Colorado River Dome). In addition, these three springs exhibit an order of magnitude lower range of ^{3}He and ^{4}He concentrations than those observed in the other springs and wells (Fig. 4).

4.3. Neon

The lowest ^{20}Ne concentrations are those observed in the deep CO_2 gas wells, which are typically two orders of magnitude lower than all of the other water samples. The increase in ^{20}Ne corresponds to moving southeast within the CO_2 reservoir towards the gas/formation water contact. As ^{20}Ne is primarily derived from the atmosphere this indicates the increased interaction between the CO_2 and the formation water. $^{20}Ne/^{22}Ne$ values within these samples are within error of the air value of 9.80 and $^{21}Ne/^{22}Ne$ values range from 0.0408 to 0.0446, significantly higher than the air value of 0.0290. This can be explained as the result of mixing between a pre-mixed crust/mantle component and air (Gilfillan et al., 2008).

^{20}Ne concentrations within the water samples show no distinct variation between any of the sample types. These concentrations are at least an order of magnitude higher than air saturated water (ASW) (assuming a 10% excess air component) of 1.89×10^{-7} cm^3 STP cm^{-3} with many of the values also being above the air concentration of 1.65×10^{-5} cm^3 STP cm^{-3}. The majority of the water samples also show clear deviation from the $^{20}Ne/^{22}Ne$ air value, with values ranging from 9.81 ± 0.02 to 10.05 ± 0.02. This excess ^{20}Ne can be explained by a mass fractionation process similar to that documented observed in the San Juan Basin methane gas field (Zhou et al., 2005) and at the Green River Springs (Wilkinson et al., 2010). $^{21}Ne/^{22}Ne$ ratios from the water samples are all within error of the air value of 0.0290.

4.4. Argon

^{40}Ar concentrations within the three deep CO_2 gas samples are well below the air value of 9.30×10^{-3} cm^3 STP cm^{-3}. ^{40}Ar concentrations correlate directly with ^4He and ^{20}Ne on moving southeast within the CO_2 reservoir closer to the gas/formation water contact. ^{36}Ar concentrations also increase with proximity to the gas/formation water contact. Measured $^{40}Ar/^{36}Ar$ ratios range from 1369 ± 13 to 1687 ± 17, significantly above the air value of 295.5, as a result of a resolvable excess of ^{40}Ar ($^{40}Ar^*$). Measured $^{38}Ar/^{36}Ar$ ratios are above the air value of 0.188 indicating addition of radiogenic ^{38}Ar as documented in Ballentine and Burnard (2002).

The water samples all exhibit ^{40}Ar concentrations that are slightly in excess of the air value. Measured $^{40}Ar/^{36}Ar$ ratios are also slightly in excess of the air ratio ranging from 296 ± 0.6 to 307 ± 0.6. As with the CO_2 gas samples this is the result of a small excess of radiogenic ^{40}Ar, however, it is clear that almost all of the ^{40}Ar in the samples is air derived. The majority of the measured $^{38}Ar/^{36}Ar$ values in the water samples are also within error of the air value. However, two of the spring samples and two of the well samples exhibit ratios that are in excess of the air value. This is probably the result of the addition of crustal derived ^{38}Ar (Ballentine and Burnard, 2002).

5. Discussion

It is readily apparent from both He and Ne data that the three anomalous spring samples (Willowbank Spring, 24 Bar Ranch and New Mexico Spring) stand out markedly from the other surface springs and groundwater wells sampled. These three surface springs Exhibit $^3He/^4He$ ratios in excess of the air value (Figs. 2b and 4) and dramatically lower $^4He/^{20}Ne$ ratios than those observed in the other water samples (Fig. 3). Hence, the key question to answer is whether these differences can be proven to be due to a lack of contact with CO_2 migrating from the reservoir. To answer this question we now focus on comparing the noble gas measurements with both stable isotope and water chemistry data.

5.1. Relationship of HCO_3^- to $\delta^{13}C$ and $^3He/^4He$

Measurements of $\delta^{13}C$ have been extremely valuable in tracing CO_2 injected into early CO_2 storage test sites (Fessenden et al., 2010; Krevor et al., 2010, 2011; Leuning et al., 2008; Raistrick et al., 2006). However, at the St Johns site no clear relationship between the HCO_3^- content of the water and the $\delta^{13}C_{DIC}$ ratio or sample type exists (Fig. 2a). This is unsurprising given that there are many CO_2 sources in the crust, with each source exhibiting $\delta^{13}C$ isotope ranges which are not discrete (Wycherley et al., 1999). This is in stark contrast to the systematic relationship between HCO_3^- concentration and $^3He/^4He$, which illustrates a distinction between the above atmospheric ratios measured in the three anomalous spring water samples, and the significantly below atmosphere $^3He/^4He$ measured in all of the other samples (Fig. 2b). All of the other water samples have higher HCO_3^- concentrations which correspond to lower $^3He/^4He$ ratios and represent a trend towards the $^3He/^4He$ and HCO_3^- values recorded in the deep CO_2 well water (Fig. 2b).

5.2. ^4He and ^3He concentrations

There is no significant source of He within the atmosphere as it is lost by diffusion to space (Ballentine et al., 2002). ^4He predominantly originates from the radioactive decay of U and Th in the crust and accumulates in deep formation waters over time (Torgersen and Clarke, 1985). Hence, the significantly higher than atmosphere concentrations of ^4He in all of the groundwater wells and majority of surface springs implies the addition of a crustal component which has accumulated radiogenic ^4He over time (Gilfillan et al., 2008). This indicates that a portion of the water contained in the springs and wells in the St. Johns area has originated at depth (Torgersen and Clarke, 1985). The ^4He excess is further shown by the significantly above atmosphere $^4He/^{20}Ne$ ratios in all of the groundwater wells and majority of surface springs, excluding the anomalous springs (Fig. 3). Fig. 4a illustrates that the low $^3He/^4He$ and high ^4He within the groundwater wells and majority of surface springs (except for the anomalous springs) can be explained by simple mixing between deep well water, which exhibits low $^3He/^4He$ ratios and high ^4He values, and varying amounts of shallow groundwater that has an atmospheric $^3He/^4He$ ratio and ^4He concentration. This illustrates that the excess ^4He fingerprint entrained at depth is retained on migration of the waters to the surface.

^3He in the subsurface predominantly originates from the mantle (Ballentine and Burnard, 2002). The $CO_2/^3He$ ratios from St. Johns are within the magmatic (MORB) range of $1–10 \times 10^9$ identifying a primary magmatic origin of the CO_2 (Burnard et al., 1997; Gilfillan et al., 2008). As with ^4He, the low $^3He/^4He$ and associated high ^3He within the deep groundwater wells and most surface springs, can be explained by simple mixing between water from wells 10-22 and 22-1X and the atmosphere (Fig. 4b). Consequently, all of the ^3He rich waters must have interacted to some degree with the deep reservoir magmatic CO_2. This illustrates that the fingerprint of high ^3He, from magmatic origin contained in the deep CO_2 wells, although diluted, is retained during transport of water and CO_2 to the surface.

5.3. ^{40}Ar and ^{36}Ar concentrations

^{40}Ar and ^{36}Ar concentrations are slightly above the air concentration in all of the water samples. This excess Ar can be attributed to the addition of a small radiogenic component. $^{40}Ar/^{36}Ar$ ratios vary slightly between the spring water samples and the groundwater wells (293–299 and 298–307) but there is no significant difference between the majority of the samples and the three anomalous springs. As both Ar concentrations and $^{40}Ar/^{36}Ar$ ratios are similar for all samples it is clear that Ar is not a useful tracer of CO_2 interaction in this study. This is unsurprising given the high proportion of Ar in the atmosphere which explains why all the water samples are dominated by atmospheric Ar contributions.

5.4. $CO_2/^3He$ ratios and relationship to ^{20}Ne and ^4He

All waters, except for the three anomalous springs, exhibit $CO_2/^3He$ ratios which are extremely similar to those observed in the three deep CO_2 wells (Fig. 5). It is important to note that the dissolved CO_2 concentrations are calculated maximum values under subsurface conditions which do not take any CO_2 degassing from the waters during migration into account (see Section 3). Hence, the $CO_2/^3He$ ratios are calculated maximum values, yet none, aside from the three from the anomalous springs, are above the range observed in deep reservoir CO_2 samples. These results further reinforce that all of the water samples, except the anomalous springs, contain CO_2 of magmatic origin, which has originated from the CO_2 reservoir. The higher $CO_2/^3He$ ratios observed in the three anomalous springs indicates they contain CO_2 with less ^3He than the deep reservoir, providing further evidence that they contain CO_2 from a different, non magmatic source. The small amount of ^3He from tritium decay does not significantly alter $CO_2/^3He$ in these samples. Several samples exhibit ratios below the lowest observed CO_2 well value of 9.75×10^7, implying that some CO_2 component has been lost relative to ^3He, possibly as a result of mineral precipitation or degassing.

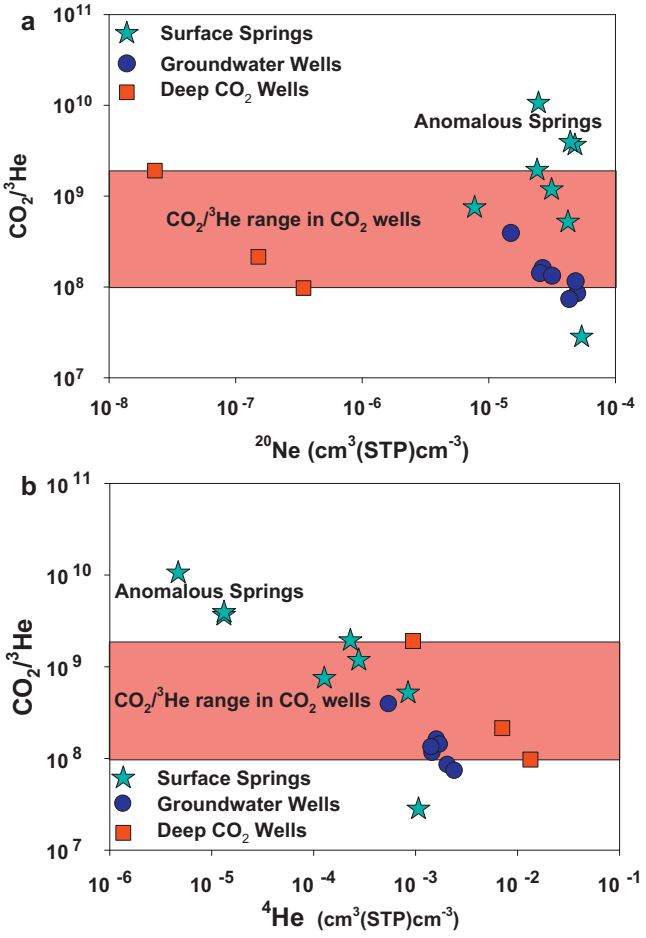

Fig. 5. (a) $CO_2/^3He$ variation plotted against ^{20}Ne. All of the groundwater springs and the majority of the surface springs exhibit $CO_2/^3He$ ratios which are extremely similar to those measured in the deep CO_2 wells, implying that they contain dissolved CO_2 which has migrated from the CO_2 reservoir. There is a clear trend of decreasing $CO_2/^3He$ with increasing ^{20}Ne in all of the data. As ^3He is a conservative tracer, reduction of $CO_2/^3He$ can only be explained by a reduction of the CO_2 component. As the groundwater is the main source of ^{20}Ne, this CO_2 reduction must be linked to contact with the groundwater. (b) $CO_2/^3He$ variation plotted against ^4He. Again there is a clear reduction in the $CO_2/^3He$ ratio that corresponds to an increase in ^4He. This is the result of the ^4He, which has accumulated in the deep formation water, mixing with the younger shallow groundwater and then migrating from the reservoir, along with dissolved CO_2. This trend is identical to that observed in natural CO_2 reservoirs from around the world (Gilfillan et al., 2009).

There is a clear relationship between $CO_2/^3He$ reduction and increases in both ^{20}Ne and especially ^4He (Fig. 5a and b) and similar relationships have been observed in numerous CO_2 reservoirs from around the world (Gilfillan et al., 2009; Sherwood Lollar and Ballentine, 2009). ^{20}Ne is introduced into the subsurface as a component of air dissolved in water and, hence, is a useful tracer of groundwater interaction (Ballentine et al., 2002). Whilst there are means by which crustal CO_2 ($CO_2/^3He > 10^{10}$) could be added to an initial mantle rich CO_2 accumulation (Bradshaw et al., 2004; Cathles and Schoell, 2007), there is no plausible mechanism that would permit crustal CO_2 to be added whilst preserving the correlation between $CO_2/^3He$ reduction and increases in noble gases derived from the groundwater. Therefore, changes in $CO_2/^3He$ must be due to CO_2 loss in the subsurface by an amount directly related to the quantity of groundwater the CO_2 has contacted. As CO_2 is soluble and reactive, the most probable mechanisms of subsurface CO_2 fluid phase removal are dissolution of the CO_2 into the groundwater and/or mineral trapping (Baines and Worden, 2004; Bradshaw et al., 2004). In some natural CO_2 reservoirs it has been possible to distinguish between proportions of CO_2 dissolving into the formation water and those precipitating as carbonate minerals (Gilfillan et al., 2009). However, due to the lack of correlation between the $\delta^{13}C$ and $CO_2/^3He$ this is not possible in these waters.

5.5. Potential of noble gases to trace the migration of stored anthropogenic CO_2

The noble gas measurements from groundwater springs in the St. Johns region imply that deep natural CO_2 is dissolving into the reservoir formation water, a process that has been previously documented in natural gas reservoirs from around the world (Gilfillan et al., 2009). This formation water containing dissolved CO_2 is then migrating through the shallow groundwater to the surface, as highlighted by the elevated concentrations of both ^3He and ^4He measured in the majority of the spring waters. As previously outlined, ^4He originates in the crust from the radiogenic decay of U and Th and accumulates in the formation water over time. The atmosphere contains very little He as it is not retained by the Earth's gravitational field (Ballentine et al., 2002) and therefore any air component entrained in captured anthropogenic CO_2 will only contain a minimal amount of ^4He and virtually no ^3He.

The most probable storage sites for anthropogenic CO_2 will be in the porespace of depleted hydrocarbon fields or saline aquifers, both of which also contain natural formation water. Should the stored CO_2 dissolve into the formation water and then subsequently migrate to the surface, the dissolved CO_2 will inherit the ^4He signature of the formation water, which in natural US CO_2 reservoirs has been found to be 10–1000 times higher than the ^4He concentration of air (Gilfillan et al., 2009). Therefore, identification of elevated ^4He concentrations in CO_2 rich near surface water samples surrounding an engineered storage site would imply migration of a portion of injected CO_2 to the surface. Hence, measurements of ^4He and dissolved CO_2, using similar methods to those outlined in this study, have the potential to identify the migration of dissolved anthropogenic CO_2 from a deep storage site.

Additionally, the preservation of the magmatic ^3He fingerprint, which originates directly from the natural CO_2, in the surface water

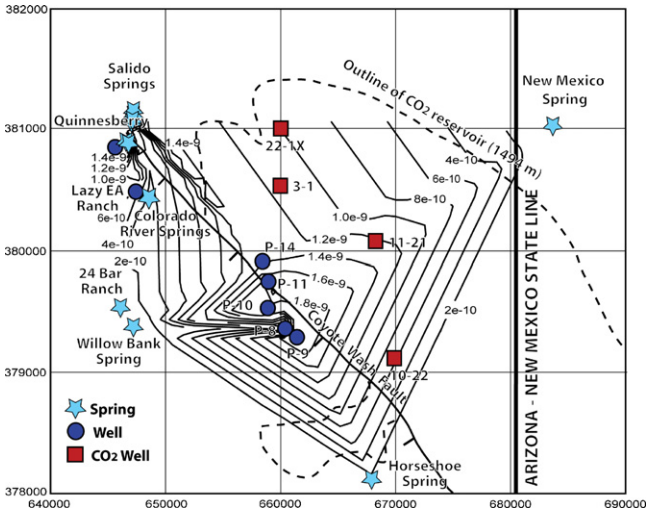

Fig. 6. Diagrammatic contour plot of ^3He concentrations plotted from measurements from the groundwater wells and surface springs. The positions of CO_2 wells are shown for reference only. As ^3He predominantly originates from the mantle, the high ^3He concentrations measured in water samples located along the fault trace and at the northern fault tip of the Coyote Wash fault at Salido Springs can only be explained by the presence of water rich in magmatic CO_2 in these areas. This strongly implies that migration along the fault, or its damage zone, is the means by which magmatic CO_2 rich water containing ^3He is reaching the surface.

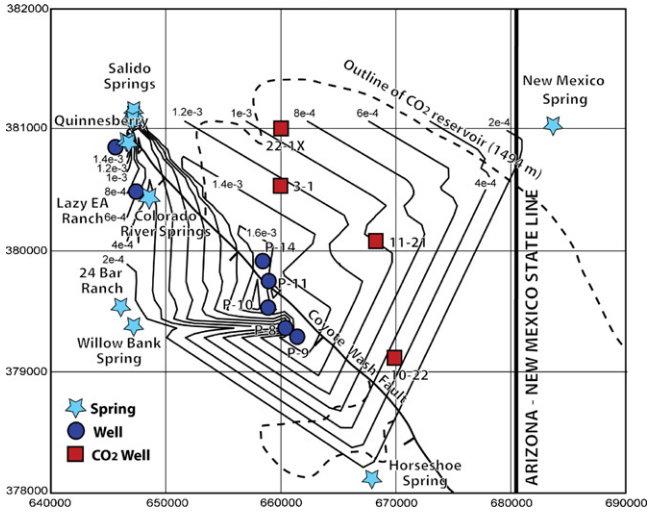

Fig. 7. Diagrammatic contour plot of ^{4}He concentrations plotted from measurements from the groundwater wells and surface springs. The positions of CO_2 wells are shown for reference only. As ^{4}He predominantly originates from the crust, the high ^{4}He concentrations measured in water samples located along the fault trace and at the northern fault tip of the Coyote Wash fault at Salido Springs can only be explained by the presence of water which has originated from depth and is rich in radiogenic ^{4}He. This further implies that migration along the fault, or its damage zone, is the means by which this deep water containing ^{4}He is reaching the surface.

samples indicates that an artificial noble gas fingerprint, created by the addition of Kr or Xe to injected anthropogenic CO_2, would also be preserved. This lays the foundation for the use of similar noble gas tracing techniques as tools to identify dissolved CO_2 migration from engineered storage sites.

6. Conclusions

Our results illustrate that He and Ne concentrations and ^{3}He/^{4}He, ^{4}He/^{20}Ne and CO_2/^{3}He ratios provide characteristic isotope ratio fingerprints which have been measured in all of the groundwater wells and all but three of the surface springs. This can only be explained if the sampled shallow well and spring waters contain noble gases together with magmatic CO_2 derived from the deep reservoir. This proves that high concentrations of HCO_3^- present in sampled waters are the direct result of the migration of dissolved CO_2 from the deep reservoir.

High ^{3}He and ^{4}He abundances are measured in water samples located along the fault trace and at the northern fault tip of the Coyote Wash fault at Salido Springs (Figs. 6 and 7). This strongly implies that migration along the fault, or its damage zone, is the means by which CO_2 rich water is reaching the surface. This illustrates, for the first time, that CO_2 can be fingerprinted from source to surface using noble gases, particularly He. This paves the way for the use of similar techniques to identify dissolved CO_2 migration from engineered storage sites.

Acknowledgements

S.M.V.G. was supported by a Natural Environmental Research Council (NERC) funded Postdoctoral position, grant NE/C516479/1 and a NERC Postdoctoral Fellowship, grant NE/G015163/1. We thank N. Burnside for assistance and support in the field, Jeff Hammond from Tuscon Electric Power Company for providing access to the Power Station wells and Joel Quisenberry for providing access to wells on his ranch and Lazy Ea ranch.

References

Allis, R., Bergfeld, D., Moore, J., McClure, K., Morgan, C., Chidsey, T., Heath, J.E., McPherson, B., 2005. Implications of results from CO_2 flux surveys over known CO_2 systems for long-term monitoring. In: Fourth Annual Conference on Carbon Capture and Sequestration, DOE/NETL.

Baars, D.L., 2000. The Colorado Plateau: A Geologic History. University of New Mexico Press.

Baer, J.L., Rigby, J.K., 1978. Geology of the Crystal Geyser and environmental implications of its effluent, Grand County, Utah. Utah Geological and Mineral Survey Utah Geology, 125–130.

Baines, S.J., Worden, R.H., 2004. The long term fate of CO_2 in the subsurface: natural analogues for CO_2 storage. In: Bains, S.J., Worden, R.H. (Eds.), Geological Storage of Carbon Dioxide. Geological Society, London, pp. 59–85.

Ballentine, C.J., 1991. He, Ne and Ar Isotopes as Tracers in Crustal Fluids, Earth Sciences. University of Cambridge, Cambridge, UK.

Ballentine, C.J., Burgess, R., Marty, B., 2002. Tracing fluid origin, transport and interaction in the crust. In: Porcelli, D.R., Ballentine, C.J., Weiler, R. (Eds.), Noble Gases in Geochemistry and Cosmochemistry. , pp. 539–614.

Ballentine, C.J., Burnard, P.G., 2002. Production, release and transport of noble gases in the continental crust. In: Porcelli, D.R., Ballentine, C.J., Weiler, R. (Eds.), Noble Gases in Geochemistry and Cosmochemistry. , pp. 481–538.

Ballentine, C.J., Schoell, M., Coleman, D., Cain, B.A., 2001. 300-Myr-old magmatic CO_2 in natural gas reservoirs of the west Texas Permian basin. Nature 409, 327–331.

Benson, S.M., Hepple, R., 2005. Prospects for early detection and options for remediation of leakage from CO_2 storage projects. In: Benson, S.M. (Ed.), Carbon Dioxide Capture for Storage in Deep Geologic Formations. Elsevier, pp. 1189–1203.

Bradshaw, J., Boreham, C., La Pedalina, F., 2004. Storage retention time of CO_2 in sedimentary basins; examples from petroleum systems. In: Rubin, E., Keith, D., Gilboy, C. (Eds.), Greenhouse Gas Control Technologies, 7th International Conference on Greenhouse Gas Control Technologies. Vancouver, pp. 541–550.

Burnard, P., Graham, D., Turner, G., 1997. Vesicle-specific noble gas analyses of "Popping Rock": implications for primordial noble gases in Earth. Science, 568–570.

Castro, M.C., Goblet, P., 2003. Calibration of regional groundwater flow models: working toward a better understanding of site-specific systems. Water Resources Research 39, 1172.

Castro, M.C., Goblet, P., Ledoux, E., Violette, S., de Marsily, G., 1998. Noble gases as natural tracers of water circulation in the Paris Basin 2 Calibration of a groundwater flow model using noble gas isotope data. Water Resources Research 34, 2467–2483.

Cathles, L.M., Schoell, M., 2007. Modeling CO_2 generation, migration and titration in sedimentary basins. Geofluids 7, 441–450.

Craig, H., Lupton, J.E., Horibe, Y., 1978. A mantle helium component circum Pacific volcanic gases. In: Alexander, E.C., Ozima, M. (Eds.), Terrestrial Rare Gases. Japan Science Societies Press, Tokyo, pp. 3–16.

Crumpler, L.S., Aubele, J.C., Condit, C.D., 1994. Volcanoes and neotectonic characteristics of the Springerville volcanic field, Arizona. In: Chamberlain, R.M., Kues, B.S., Cather, S.M., Barker, J.M., McIntosh, W.C. (Eds.), New Mexico Geological Society Guidebook; 45th Field Conference. Mogollen Slope, West-Central New Mexico and East Central Arizona, pp. 147–164.

Dockrill, B., Shipton, Z.K., 2010. Structural controls on leakage from a natural CO_2 geologic storage site: Central Utah, U.S.A. Journal of Structural Geology 32, 1768–1782.

Doelling, H., 1994. Tufa deposits in west Grand County. County Survey Notes Utah Geological Survey, 2–3.

E.U., 2009. Directive 2009/31/EC of the European Parliament and of the Council on the geological storage of carbon dioxide. Official Journal of the European Union L140, 114–136.

Fessenden, J., Clegg, S., Rahn, T., Humphries, S., Baldridge, W., 2010. Novel MVA tools to track CO_2 seepage, tested at the ZERT controlled release site in Bozeman, MT. Environmental Earth Sciences 60, 325–334.

Gilfillan, S.M.V., Ballentine, C.J., Holland, G., Sherwood Lollar, B., Stevens, S., Schoell, M., Cassidy, M., 2008. The noble gas geochemistry of natural CO_2 gas reservoirs from the Colorado Plateau and Rocky Mountain provinces, USA. Geochimica et Cosmochimica Acta 72, 1174–1198.

Gilfillan, S.M.V., Lollar, B.S., Holland, G., Blagburn, D., Stevens, S., Schoell, M., Cassidy, M., Ding, Z., Zhou, Z., Lacrampe-Couloume, G., Ballentine, C.J., 2009. Solubility trapping in formation water as dominant CO_2 sink in natural gas fields. Nature 458, 614–618.

Happell, J.D., ÖStlund, G., Mason, A.S., 2004. A history of atmospheric tritium gas (HT) 1950–2002. Tellus B 56, 183–193.

Krevor, S., Perrin, J.-C., Esposito, A., Rella, C., Benson, S., 2010. Rapid detection and characterization of surface CO_2 leakage through the real-time measurement of [delta]13 C signatures in CO_2 flux from the ground. International Journal of Greenhouse Gas Control 4, 811–815.

Krevor, S.C.M., Ide, T., Benson, S.M., Orr, F.M., 2011. Real-time tracking of CO_2 injected into a subsurface coal fire through high-frequency measurements of the $13CO_2$ signature. Environmental Science & Technology 45, 4179–4186.

Lafortune, S., Moreira, M., Agrinier, P., Bonneville, A., Schneider, H., Catalette, H., 2009. Noble gases as tools for subsurface monitoring of CO_2 leakage. Energy Procedia 1, 2185–2192.

Leuning, R., Etheridge, D., Luhar, A., Dunse, B., 2008. Atmospheric monitoring and verification technologies for CO_2 geosequestration. International Journal of Greenhouse Gas Control 2, 401–414.

McCrea, J.M., 1950. On the isotopic chemistry of carbonates and a paleotemperature scale. Journal of Physical Chemistry 18, 849–857.

Moore, J., Adams, M., Allis, R., Lutz, S., Rauzi, S., 2005. Mineralogical and geochemical consequences of the long-term presence of CO_2 in natural reservoirs: an example from the Springerville–St. Johns Field, Arizona, and New Mexico, U.S.A. Chemical Geology 217, 365.

Nimz, G.J., Hudson, G.B., 2005. The use of noble gas isotopes for monitoring leakage of geologically stored CO_2. In: Thomas, D.C., Benson, S.M. (Eds.), Carbon Dioxide Capture for Storage in Deep Geologic Formations. Elsevier, pp. 1113–1128.

Parkhurst, D.L., Appelo, C.A.J., 1999. User's guide to PHREEQC (version 2) – a computer program for speciation, batch-reaction, one-dimensional transport and inverse geochemical calculations. U.S. Geological Survey Water Resources Investigations Report 99-4259, p. 312.

Poreda, R.J., Farley, K.A., 1992. Rare gases in Samoan xenoliths. Earth and Planetary Science Letters 113, 129–144.

Raistrick, M., Mayer, B., Shevalier, M., Perez, R.J., Hutcheon, I., Perkins, E.H., Gunter, W.D., 2006. Using chemical and isotopic data to quantify ionic trapping of carbon dioxide in oil field brines. Environmental Science and Technology 40, 6744–6749.

Rauzi, S.L., 1999. Carbon dioxde in the St. Johns–Springerville Area, Apache County, Arizonia. Arizonia Geological Survey, Open-File Report 99-2.

Sherwood Lollar, B., Ballentine, C.J., 2009. Insights into deep carbon derived from noble gases. Nature Geoscience 2, 543–547.

Sherwood Lollar, B., Ballentine, C.J., O'Nions, R.K., 1997. The fate of mantle-derived carbon in a continental sedimentary basin: Integration of C/He relationships and stable isotope signatures. Geochimica et Cosmochimica Acta 61, 2295–2308.

Sherwood Lollar, B., O'Nions, R.K., Ballentine, C.J., 1994. Helium and neon isotope systematics in carbon dioxide-rich and hydrocarbon-rich gas reservoirs. Geochimica et Cosmochimica Acta 58, 5279.

Sirrine, G.K., 1956. Geology of the Springerville–St. Johns area, Apache County Arizona. University of Texas, Austin, p. 248.

Stevens, S.H., Fox, C., White, T., Melzer, S., 2006. Natural CO_2 analogs for Carbon Sequestration. Final Report for USDOE.

Torgersen, T., Clarke, W.B., 1985. Helium accumulation in groundwater. (i). An evaluation of sources and the continental flux of crustal ^4He in the Great Artesian Basin, Australia. Geochimica et Cosmochimica Acta 49, 1211–1218.

Wildenborg, A.F.B., Leijnse, A.L., Kreft, E., Nepveu, M.N., Obdam, A.N.M., Orlic, B., Wipfler, E.L., van der Grift, B., van Kesteren, W., Gaus, I., Czernichowski-Lauriol, I., Torfs, P., Wójcik, R., 2005. Risk Assessment Methodology for CO_2 Storage: The Scenario Approach, Carbon Dioxide Capture for Storage in Deep Geologic Formations. Elsevier Science, Amsterdam, pp. 1293–1316.

Wilkinson, M., Gilfillan, S.M.V., Haszeldine, R.S., Ballentine, C.J., 2010. Plumbing the depths: testing natural tracers of subsurface CO_2 origin and migration, Utah. In: Grobe, M., Pashin, J.C., Dodge, R.L. (Eds.), Carbon Dioxide Sequestration in Geological Media – State of the Science. AAPG Studies.

Wycherley, H., Fleet, A., Shaw, H., 1999. Some observations on the origins of large volumes of carbon dioxide accumulations in sedimentary basins. Marine and Petroleum Geology 16, 489–494.

Zhou, Z., Ballentine, C.J., Kipfer, R., Schoell, M., Thibodeaux, S., 2005. Noble gas tracing of groundwater/coalbed methane interaction in the San Juan Basin, USA. Geochimica et Cosmochimica Acta 69, 5413–5428.